Journal of Alloys and Compounds 881 (2021) 160442

Contents lists available at ScienceDirect

Journal of Alloys and Compounds

journal homepage: www.elsevier.com/locate/jalcom

A porous SiC/C composite material constructed by the ordered mesoporous SiC interfacing with the ordered mesoporous carbon and its supercapacitor performance

Xinyue Liu[a,b,1], Hongwei Zhao[a,b,1], Shan Jiang[a,b], Shuai Wu[a,b], Tong Zhao[a,b], Lixiang Li[a,b,*], Xin Geng[a,b], Haiming Yang[a,b], Weimin Zhou[a,b], Chengguo Sun[a,b], Yiqing Chen[c,**], Baigang An[a,b,*]

[a] School of Chemical Engineering, University of Science and Technology Liaoning, 185 Qianshanzhong Road, Anshan 114051, China
[b] Key Laboratory of Energy Materials and Electrochemistry Research Liaoning Province, University of Science and Technology Liaoning, 185 Qianshanzhong Road, Anshan 114051, China
[c] State Key Laboratory of Metal Material for Marine Equipment and Application, Anshan 114009, China

ARTICLE INFO

Article history:
Received 5 March 2021
Received in revised form 25 April 2021
Accepted 13 May 2021
Available online 21 May 2021

Keywords:
Ordered mesopores
Interfaced pores
SiC
Magnesiothermic reduction reaction
Supercapacitor

ABSTRACT

Both SiC and porous carbons have been widely used in the fields of catalysts, ceramics, electrode materials and electromagnetic materials since their advantages of excellent chemical and thermal stability, good conductivity, flexibility and stiffness. However, pore construction of SiC still faces considerable difficulty comparing to carbon materials with a large variety of pores. Herein, by developing a novel method combining the silanization of SBA-15 template, acetylene CVD and magnesiothermic reduction reaction (MRR) technology, a novel porous material of OM-SiC@OMC that the ordered mesoporous SiC interfaces with the ordered mesoporous carbon has been successful synthesized. The silanization enhances the activity of carbon deposition into the pores of SBA-15 template, MRR results in the formation of SiC between the interface of SiO_2 and carbon. After the template removal, a novel mesoporous composite material of OM-SiC@OMC has been successfully obtained. Interestingly, OM-SiC@OMC contains two types of ordered mesopores interfacing with each other by the pore wall of SiC phase and carbon phase, respectively. As electrode materials of supercapacitors, OM-SiC@OMC exhibits a capacitance of 194.8 F g^{-1} with an excellent retention rate of 97.8% after 10,000 cycles. The present study explores a novel ordered porous materials constructed by the interfaced pores of carbon and carbide, it is promising to find good applications of these multi-interfaced porous materials.

1. Introduction

Silicon carbides (SiC) have many fascinating physical properties of excellent chemical and thermal stability, high hardness, outstanding oxidation and corrosion resistance, and low electrical resistivity and thus are promising materials for many applications [1–5]. Porous SiC has been widely used in catalyst supports, porous ceramics and gas sensors [6–11]. Most recently, porous SiC has also exhibited its potential in the electrode materials of lithium ion batteries and supercapacitor [12–16]. Using Ag coated porous AAO substrate as collector, Sanger et al., synthesized SiC nano-cauliflowers (NCs) by performing a DC magnetron co-sputtering [17]. The obtained SiC NCs exhibited a capacity of 188 F g^{-1} at 5 mV s^{-1} with good cycling stability in 1 M Na_2SO_4 solution. Kim et al., prepared porous SiC containing micro-, meso- and macropores at 1250 °C, which has a capacity of 336.5 F g^{-1} in 1 M Na_2SO_4 electrolyte at a scan rate of 5 mV s^{-1} [18]. The advantages of SiC is much better demonstrated by an all solid-state micro-supercapacitors based on SiC nanowire, at temperatures above 450 °C which can supply a high areal capacitance of 92 μF cm^{-2} with a retention of over 60% after 10,000 cycles [19]. However, it still faces considerable difficulties in synthesizing, constructing and tuning pore structure of SiC since their high stiffness and characteristic of covalent bonds between

* Corresponding authors at: School of Chemical Engineering, University of Science and Technology Liaoning, 185 Qianshanzhong Road, Anshan 114051, China
** Corresponding author.
E-mail addresses: lxli2005@126.com (L. Li), chenyiqing2003@163.com (Y. Chen), bgan@ustl.edu.cn (B. An).
[1] X.Y. Liu and H.W. Zhao equally contributed to this work.

https://doi.org/10.1016/j.jallcom.2021.160442
0925-8388/

silicon atom and carbon atom. Common routes to prepare porous SiC are carbothermal reduction of silica and the pyrolysis of precursors containing organic silicon [20–22]. These methods are complicated process, energy waste and high cost. And it is still difficult to construct and control pore structure and size of porous SiC.

Compared to carbides, porous carbons with diverse morphology and structure, such as activated carbons, fullerenes, carbon nanotubes (CNTs), graphenes, template carbons etc., have been widely developed in many fields [23–30]. Owing to structure tunability, carbon materials have much more diversity and novelty in pore structure and size than other materials. Amorphous carbons, graphitized carbons, ordered porous carbons, hierarchical porous carbons have been successfully prepared. Direct carbonization or pyrolysis of carbon containing precursors at high temperature and post-treatments are common methods to prepare porous carbons and tune their pore structure, but the pores as obtained are tedious, disordered distribution and difficult to tune [31–33]. In contrast, template carbons are the replicas of molecular sieves like SBA-15 and thus own an ordered pore structure and a focused pore size. The microporous, mesoporous and macroporous carbons with the ordered pore structure in three-dimensions have been synthesized by template methods. Therefore, template method becomes one of the most widely used technologies to design structure and control pore size of carbon. Aligned CNTs, three-dimensional graphene networks and ordered porous carbon have been synthesized using AAO, nickel foam, SBA-15 and zeolite as templates and exhibit good performance in many fields, especially in the energy storage and conversion system of battery, supercapacitor and fuel cell [34–44]. It could be a feasible route using the template containing silica to prepare and construct porous SiC.

Previously, our groups developed a method to deposit carbon layers into pores of the silanized SBA-15 by the direct CVD of acetylene and acetonitrile vapor, a porous carbon material with the dual ordered pores and the dual nitrogen-doped interfaces had been successfully obtained [45]. Since the carbon deposited SBA-15 contains the interfaces of SiO_2 and carbon, which could make the formation of Si or SiC at the interface through magnesiothermic reduction reaction (MRR) [46–48]. MRR can be used to prepare silicon with high purity by using silica as raw materials at temperature of 650 °C through the reaction (1) [49]. Traditional method of carbothermal reduction of silica to produce silicon requires the reaction temperature as high as 1600 °C. Therefore, MRR has significant advantages of much lower temperature to prepare silicon. When carbon phase exists to form the interface of carbon and silica, the following reaction of (2) and (3) can occur at the temperature of no less than 650 °C.

$$SiO_2(s) + Mg(s) \rightarrow Si(s) + 2MgO(s) \quad (1)$$

$$SiO_2(s) + Mg(s) + C(s) \rightarrow Si(s) + C(s) + 2MgO(s) \quad (2)$$

$$SiO_2(s) + Mg(s) + C(s) \rightarrow SiC(s) + 2MgO(s) \quad (3)$$

Since the free energy for SiC formation is lower than Si, reaction (3) is thermodynamically preferred to produce SiC. In the reaction (3), SiO_2 is initially reduced by magnesium to form Mg_2Si, and then Mg_2Si encounters carbon to form SiC by a solid state diffusion process [50]. It was also found that the larger contact area of SiO_2 and carbon results in more SiC [51].

Herein, by combining CVD of acetylene with MRR technology using the silanized SBA-15 as template, a novel porous material that the ordered mesoporous SiC interfacing with the ordered mesoporous carbon (OM-SiC@OMC) has been successfully prepared. As the electrode material of supercapacitor, this OM-SiC@OMC exhibits a specific capacitance of 194.8 F g^{-1} at 0.2 A g^{-1}. Even at the large current density of 5.0 A g^{-1}, it still keeps the capacity of 120 F g^{-1} after 10,000 cycles. To our best knowledge, it is the first report on the composite material with a novel structure of the ordered porous SiC interfacing the ordered porous carbon. It could make us utilize the advantages of both carbides and carbonaceous materials better.

2. Experimental

2.1. Chemicals and regents

Isopropyl alcohol (C_3H_8O, A. R. grade, ≥ 99.7%), Hydrochloric acid (HCl, A. R. grade, 36.0–38.0%), Potassium hydroxide (KOH, A. R. grade, ≥ 99.7%), were purchased from Sinopharm Chemical Reagent Co., Ltd. Hexamethyl disiloxane (HMDSO, $C_6H_{18}OSi_2$, 99.0%), polytetrafluoroethylene (PTFE $(C_2F_4)_n$, 60 wt%) and magnesium powder (Mg, 2 N) were obtained from Shanghai Aladdin Biochemical Technology Co., Ltd. SBA-15 (hexahedron, about 6–11 nm of pore size), was obtained from Advanced Materials Technology Co., Ltd. Hydrofluoric acid (HF, ≥ 40%) was obtained from Macklin Biotechnology Co., Ltd. Ultrapure N_2 and C_2H_2 were supplied by Anshan Angang Gas Co.,Ltd.

2.2. Material preparation

Molecular sieve of SBA-15 was used as template to prepare OM-SiC@OMC. Since the inert surface of pore walls of SBA-15 for carbon deposition, the silanization of SBA-15 was carried out to improve the activity of carbon deposition. The hexamethyl disioxane (HMDSO) (6.5 g), 2-propanol (7.5 g) and 5 M HCl (15.0 g) were mixed and stirred at 75 °C for 0.5 h and then SBA-15 powder (0.2 g) was added to the solution. The resulting biphasic mixture was vigorously stirred at 75 °C for 1.0 h and then which was filtered and dried in air at 80 °C for 5.0 h. Finally, the silanized SBA-15 was obtained.

Chemical vapor deposition (CVD) of acetylene was performed to deposite the carbon layers onto the surface of pore walls of silanized SBA-15. A certain amount of the silanized SBA-15 powder were loaded in a ceramic boat, then the powder was placed into a vertical CVD furnace. Before ascending temperature, pure nitrogen gas with a flow rate of 50 mL min^{-1} was flowed through the CVD furnace for 10 min and then the furnace was heated with a ramp of 10 °C min^{-1} in a pure nitrogen flow of 50 mL min^{-1}. Once the temperature gets to 600 °C, the high pure acetylene with a flow rate of 5 mL min^{-1} was flowed together with nitrogen gas with a flow rate of 45 mL min^{-1} into the furnace. To control the carbon layers deposited on the pore walls of the silanized SBA-15, the CVD of acetylene at 600 °C was carried out for 5.0 h. After the CVD of acetylene, the furnace was naturally cooled to the room temperature in pure nitrogen atmosphere. The samples as prepared by the CVD of acetylene are the porous composite of carbon layers coated SBA-15 and labeled as C@SiO_2.

MRR technology was used to make the interface reaction of SiO_2 phase of SAB-15 and the carbon layers to produce SiC phase. A certain amount of pure magnesium powders and C@SiO_2 were mixed and loaded in a ceramic boat, which was then moved in a muffle furnace filled with pure nitrogen gas. The furnace was ascended to 700 °C with a ramp of 10 °C min^{-1} and kept for 4.0 h. Then it was cooled to the ambient temperature in pure nitrogen atmosphere and the obtained sample was taken out. 1.0 M HCl solution was used to remove byproduct of MgO of sample. The unreacted SiO_2 was removed by 10.0 wt% HF solution. Finally the obtained sample was filtered and washed by deionized water and then dried in vacuum at 80 °C. The product is named OM-SiC@OMC.

2.3. Material characterization

Fourier-transform infrared spectra (FTIR, BRUKER Alpha, KBr pellets) of samples were collected in the range of 400–4000 cm^{-1}. X-rays diffractions (XRD, Rigaku X′pret Powder, D/MAX-2500X, Cu Kα)

were used to analyze the compostion of samples. The morphology and microstructure of samples were observed by using scan electron microscopy (SEM, FEI Apreo, operated at 1.0 kV) and transmission electron microscopy (TEM, FEI Talos F200X, operated at 200.0 kV). Nitrogen adsorption/desorption isotherms of samples were measured using a physical adsorption analyzer (Micromeritics, ASAP2020). The specific surface area (SSA) of samples was determined according to the Brunauer-Emmett-Teller (BET) method. Pore related parameters of samples were analyzed using the NLDFT model based the N_2 adsorption/desorption isotherms.

2.4. Electrochemical tests

The supercapacitor performance of OM-SiC@OMC was examined by an electrochemical analysis system (Reference 3000 workstation, Gamry Instruments, USA) and a battery tests system (ArBin BT 2000 battery). Cyclic voltammetry (CV) tests were cariried out by using a three-electrode cells where a Hg/HgO electrode and a platinum mesh with apparent surface area of 1.0 cm [2] were used as reference electrode and counter electrode, respectively. Galvanostatic charge/discharge (GCD) was tested by using a symmetric two-electrode system. Electrochemical impedance spectra (EIS) measurements were carried out at open circuit potential (OCP) with sine amplitude of 5.0 mV in frequency range of 100 kHz to 10 mHz. The working electrodes were prepared as the following process. OM-SiC@OMC, carbon black and 10.7 μL mg^{-1} PTFE binder were weighed as a mass ratio of 8:1:1 and the they were dispersed in ethanol solution and then dried in a vacuum oven at 75 °C for 3.0 h. Then an certain amount of the mixtures were uniformly dispersed onto the two pieces of nickel foam, which was pressed at a pressure of 10.0 MPa to obtain the desired working electrode plates. Before electrochemical tests, the working electrodes were immersed in 6.0 M KOH solution for 72 h to make it fully wetted by the electrolyte. The specific capacitance value (C) derived from the GCD data was calculated according to the following equation:

$$C = \frac{2}{m\Delta V} I\Delta t$$

In the equation, I is the current density of discharge, Δt is the discharge time, m is the mass of the active materials of single electrode, and ΔV is the potential window.

3. Results and discussion

Fig. 1 is a schematic diagram of preparing OM-SiC@OMC by using the silanized SBA-15 as template through the CVD of acetylene and MRR technology. FTIR spectra of SBA-15 before and after the silanization are shown in Fig. 2. The bands of Si-OH, Si-O-Si and Si-O that are inert for carbon deposition can be clearly observed around 3425, 1053 and 810 cm^{-1} for SBA-15, respectively. After the silanization these bands become weak, in addition, the new formed bands of C-H at 2998 cm^{-1} and Si-C at 841 cm^{-1} can be observed. [52–54] It confirms that the silanization makes SBA-15 matrix coupled with alkyl and Si-C band, which can bring the SBA-15 a good activity for carbon deposition.

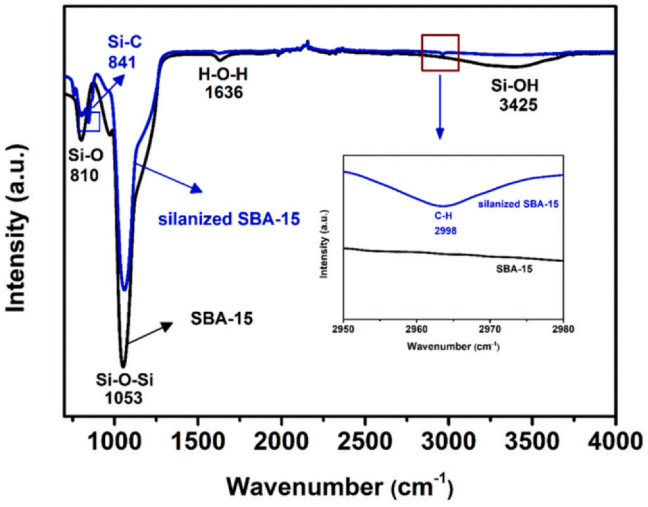

Fig. 2. FTIR of SBA-15 before and after silanization.

XRD was used to analyze the composition and structure of samples. Fig. 3(a) shows XRD patterns of samples in the small-angle diffraction. Both SBA-15 and the silanized SBA-15 show three diffraction peaks at 2θ of 0.87, 1.50 and 1.72° corresponded to the (100), (110) and (200) reflections of 2D hexagonal ordered structure, which suggests that the silanization does not change the originally ordered structure of SBA-15 [55]. Furthermore, the XRD pattern of OM-SiC@OMC also contains the peaks located at the same 2θ degree of 0.87° although the diffraction peak intensity becomes weak. It indicates that the ordered pore structure of SBA-15 is still kept after the carbon coating by the CVD, MRR and template removal. Fig. 3(b) shows the wide-angle XRD patterns of samples. Both SBA-15 and the silanized SBA-15 consist of amorphous phase of SiO_2 characterized by the diffraction peaks around 2θ of 22.8°. The resultant OM-SiC@OMC consists of β-SiC discerned by the peaks around 2θ of 35.9, 60.2 and 72.8° corresponding to the crystal face of (111), (220), (311) of SiC (JCPDS 29–1129), respectively, and carbon phase assigned to C

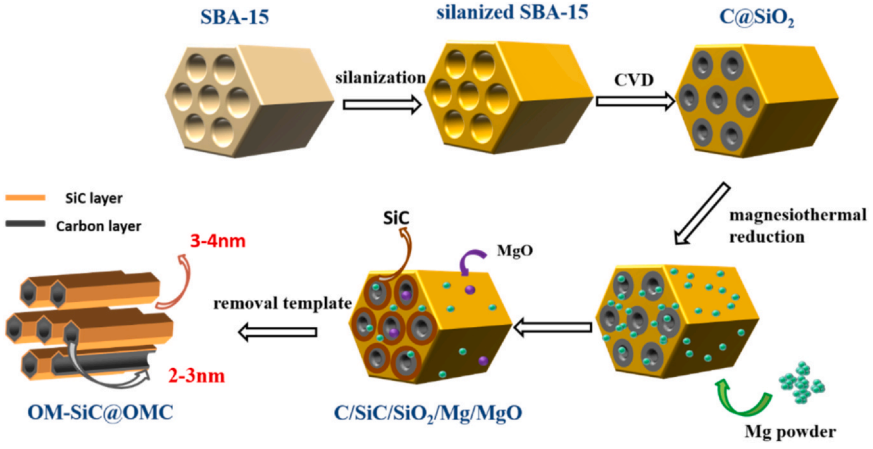

Fig. 1. Schematic diagram of preparing OM-SiC@OMC.

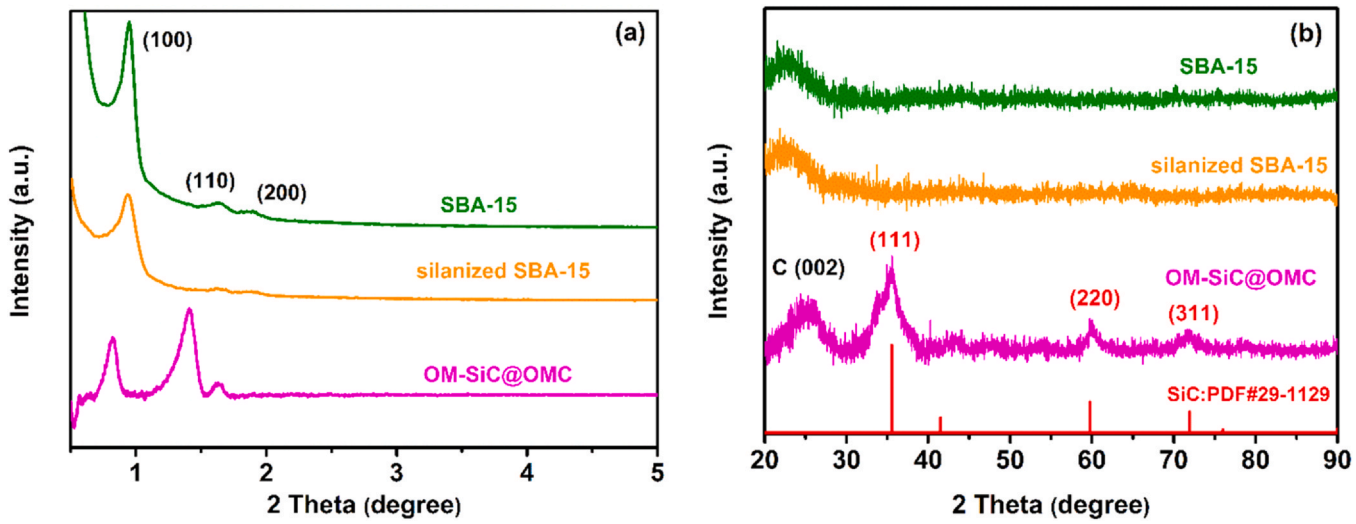

Fig. 3. XRD patterns of samples in (a) small-angle and (b) wide-angle.

(002) around 2θ of 25.1°. The formation of SiC should be attributed to the reaction of SiO_2 and carbon at the interface by MRR at 700 °C.

N_2 adsorption-desorption isotherms of samples are shown in Fig. 4(a). All the samples show the type IV isotherms with parallel H1 type hysteresis loops, indicating the characteristic of mesoporous structure of samples. However, the hysteresis loop of OM-SiC@OMC shifts to the lower relative pressure of 0.4–0.6 comparing with the SBA-15 and the silanized SBA-15 whose loops are in the relative pressure of 0.6–0.8. It suggests a decrease in the pore size of OM-SiC@OMC owing to the carbon layers coated on the wall of silanized SBA-15 template.

Pore size distribution (PSD) curves shown in Fig. 4(b) further demonstrate the evolution of pore size of samples. The original pores of SBA-15 are mainly focused on the size of from 6.5 to 7.5 nm. The silanization makes SBA-15 coupled with alkyl and Si-C band, but hardly changes the pore size and its distribution. It is worthy to note that the mesopore size of OM-SiC@OMC becomes smaller and the pore size distribution is wider. The decrease in the mesopore size is mainly attributed to the deposited carbon layers onto the surface of pore walls of the silanized SBA-15, which is consistent with the result shown by the isotherm of Fig. 4(a). The wider pore size distribution of OM-SiC@OMC is most probably attributed to the formation of two types of pores by tracing back to the preparing process. One type of mesopore is inherited from the original mesopore of SBA-15, the resultant mesopores by acetylene CVD have the smaller pore size due to the deposition of carbon layers. The other type of mesopore is produced by etching the pore walls of SBA-15. After the acetylene CVD, the MRR makes an interface reaction between the SiO_2 of SBA-15 and the carbon layers, which results in the formation of SiC. After etching the unreacted SiO_2 by HF solution, a new type of pore is formed and the pore wall is composed of SiC phase. Since OM-SiC@OMC contains two types of mesopores compared to SBA-15 only with one type of mesopore, OM-SiC@OMC owns the higher SSA of 757.4 $m^2\ g^{-1}$ than the SBA-15 template (531.9 $m^2\ g^{-1}$). For the porous materials of supercapacitor electrode, small mesopores can supply more active surface for ions accumulation, wide distribution of mesopores from pore size to pore type can facilitate the transport and diffusion of electrolyte ions. [56–60] Therefore, OM-SiC@OMC could exhibit a good performance as electrode material of supercapacitor.

As shown by SEM images of Fig. 5, both SBA-15 and OM-SiC@OMC have the cuboid-like morphologies consisted of the regular arrangement of fine rods. It means that OM-SiC@OMC is obtained by the process of silanization, CVD of acetylene, MRR and HF solution etching still inherits the apparent feature of SBA-15 well. Especially noting is that the silanization of SBA-15 successfully make the

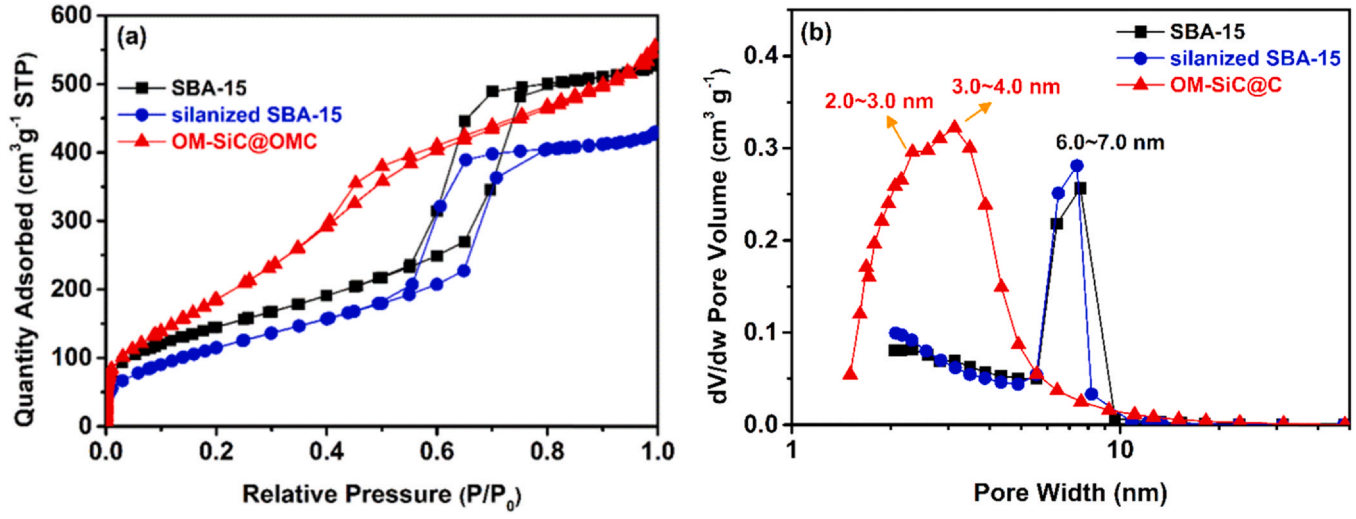

Fig. 4. (a) N_2 adsorption-desorption isotherms and (b) pore size distribution curves of samples.

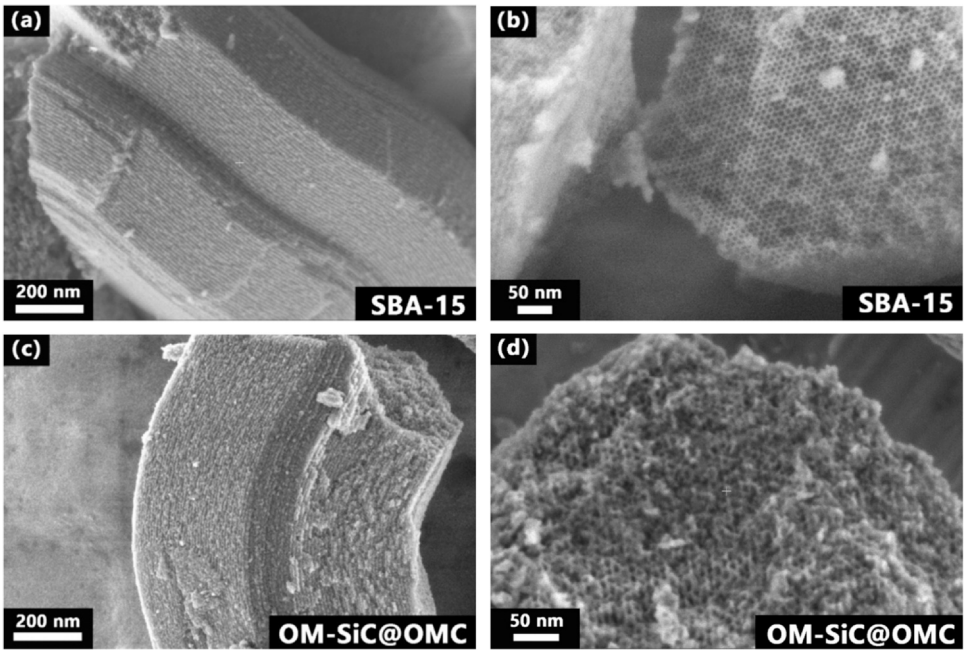

Fig. 5. SEM images of SBA-15 and OM-SiC@OMC: (a) and (c) side-view, (b) and (d) cross-sectional view.

carbon deposited onto the pore walls of template by acetylene CVD, since there are almost no carbon coatings around the eternal surface of OM-SiC@OMC particles being observed as shown by the SEM. As shown by SEM images of Fig. 5, both SBA-15 and OM-SiC@OMC demonstrate an ordered structure. Form side-view, they have the cuboid-like morphologies consisted of the regular arrangement of fine rods. From cross-sectional view, it can be observed that the pores of both samples are uniformly and ordered distribution, but the pore type and size of OM-SiC@OMC seem a little different from SBA-15.

The pore structures and arrangements of samples were further observed by high resolution TEM (HRTEM) and the results are shown in Fig. 6. The SBA-15 contains one type of cylindrical pores with size around 7.0 nm and the pore walls with the thickness of around 3.0 nm, and they are ordered arrangement from the cross-sectional and axial views of HRTEM observation. OM-SiC@OMC shows the similarity and difference in microstructure contrasted to the original SBA-15, the pores still keep the ordered arrangements like SBA-15. However, there are two types of mesopores. One type of cylindrical mesopore inherits from the SBA-15, but the pore size (2.0–3.0 nm) becomes smaller due to the carbon layers by the CVD, and the pore walls are composed of carbon. The other type is the new-formed hexagonal mesopores by etching the residual SiO_2 of the pore walls of SBA-15 and the pore width is 3.0–4.0 nm. The pore wall of this hexagonal pore is composed of SiC. EDS of OM-SiC@OMC shown in Fig. 6(e) indicates that the elements of Si, C and O are uniformly distributed around the pores of OM-SiC@OMC. The oxygen element should be produced during the removal of template by HF solution.

Combining HRTEM observation with the results of XRD and PSD, it has been well demonstrated and confirmed that OM-SiC@OMC is composed of two phases of SiC and carbon, constructed by two types of ordered mesopores. Especially interesting, these two types of mesopores interface with each other by the pore walls of SiC and carbon to produce a novel composite material that the ordered mesoporous SiC interfacing with the ordered mesoporous carbon. With our best knowledge, it is the first report about such a novel porous composite material constructed by two types of the interfaced ordered mesopores.

Generally, porous materials with a large SSA can supply a high electric double layers capacitance (EDLC) as electrode materials of supercapacitors. Since the ordered mesoporous structure with high SSA of OM-SiC@OMC, its supercapacitor performance was examined by electrochemical methods. Fig. 7(a) shows CV curves of OM-SiC@OMC in 6.0 M KOH solution with different scan rates. All CV curves show a symmetrical quasi-rectangular shape, suggesting EDLC behavior and a good charge-discharge rate property of OM-SiC@OMC, which could be attributed to the dual-ordered mesoporous structure facilitating transport of electrolyte ions. Galvanic charge-discharge (GCD) curves of OM-SiC@OMC are shown in Fig. 7(b), the curves represent by a good symmetrical triangular-shape at different currents density, suggesting the EDLC behavior and a good rate performance of the supercapacitor, which is consistent with the CV results. As shown in Fig. 7(c), OM-SiC@OMC exhibits the specific capacitance of 194.8 F g^{-1} at 0.2 A g^{-1} and can supply a capacitance of 123 F g^{-1} even at a much larger current density of 5.0 A g^{-1}. It also has a good rate performance of OM-SiC@OMC, which shows a 97.8% retention rate of capacitance at 5.0 A g^{-1} after 10,000 cycles, as shown in Fig. 7(d). Both two types of ordered mesopores of OM-SiC@OMC supply the abundant interface for charges accumulation and the channels for quick electrolyte transport, therefore OM-SiC@OMC owns a good potential as the electrode material of supercapacitor. As shown in Fig. 7(e), EIS of OM-SiC@OMC contains a semicircle in the high-frequency range and a straight line in the low frequency region, which represents a typical feature of EDLC supercapacitor. In low frequency region, the straight line has a slope close to 90° indicating a low diffusion resistance, which could be attributed to the ordered mesoporous structure of OM-SiC@OMC facilitating transport of electrolyte ions. In the high frequency region, the real axis intercept of R_s is the internal resistance including electrode and electrolyte, which is little higher than activated carbon electrode probably due to low conductivity of SiC compared to carbon materials in OM-SiC@OMC [61,62].

The specific capacitance of most activated carbons derived biomass material is in the range of 100–200 F g^{-1} [63–66]. The OM-SiC@OMC can supply the specific capacitance of 194.8 F g^{-1} at 0.2 A g^{-1} and has a good rate performance. In addition, SiC owns a strong

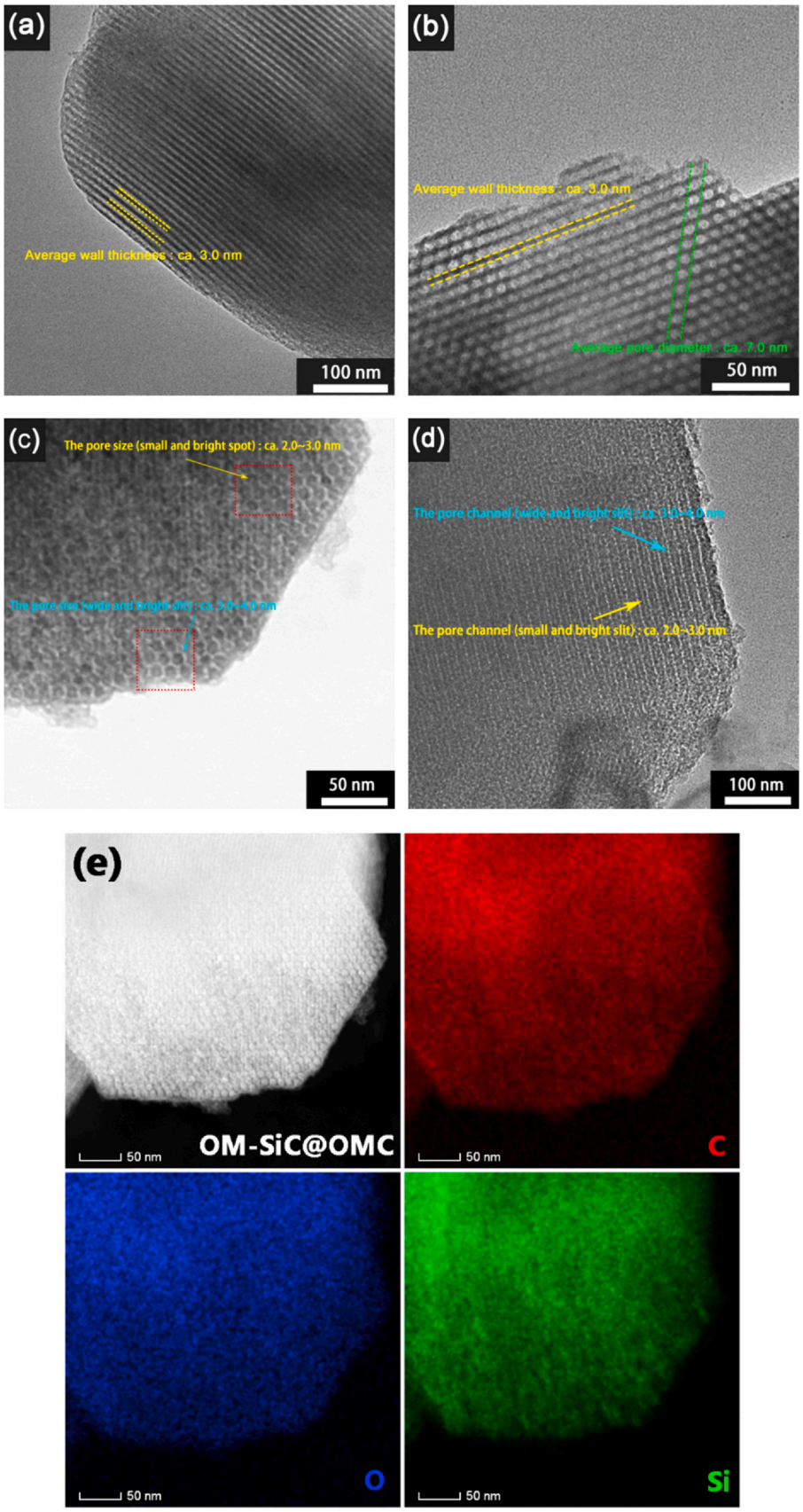

Fig. 6. TEM images of SBA-15 (a) and (b), OM-SiC@OMC of (c) and (d), (e) EDS mapping of OM-SiC@OMC.

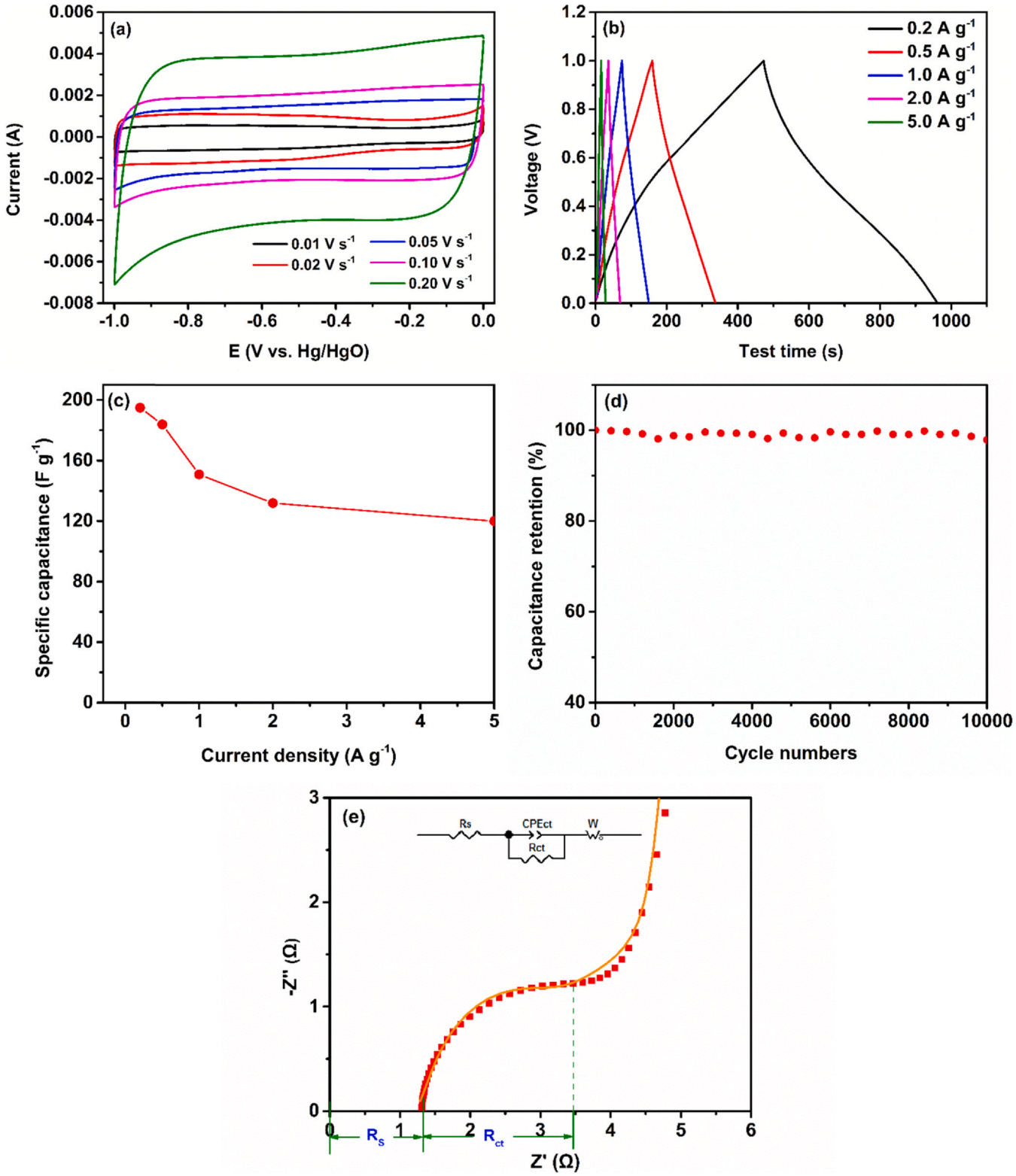

Fig. 7. (a) CV curves, (b) GCD curves, (c) rate performance, (d) cycling life and (e) EIS curves of OM-SiC@OMC.

oxidation resistance and a good thermal stablility, therefore, OM-SiC@OMC could be a good candidate for supercapacitor materials.

4. Conclusions

A novel porous material of OM-SiC@OMC that the ordered mesoporous SiC interfaces with the ordered mesoporous carbon has been successfully synthesized by developing a technical route of combination of silanizing SBA-15, CVD of acetylene and MRR. The silanization can enhance the activity of SBA-15 for carbon deposition through coupling with alkyl and Si-C band on the wall of SBA-15. Acetylene CVD results the carbon layers deposited onto the pore walls of the silanized SBA-15, which makes it possible to produce SiC through the interface reaction of the carbon layers and the SiO_2 of

template by MRR. OM-SiC@OMC contains two types of ordered mesopores, one type is cylindrical mesopores with size of 2.0–3.0 nm inherited from SAB-15, the pore wall is composed of carbon phase, the other is hexagonal mesopores with size of 3.0–4.0 nm produced through etching the unreacted SiO_2 of pore walls of SAB-15, the pore wall is composed of SiC phase. As electrode materials of supercapacitor, OM-SiC@OMC exhibits a good performance with the capacitance of 194.8 F g^{-1} at 0.2 A g^{-1}, the capacitance retention of 97.8% at 5.0 A g^{-1} after 10000 cycles.

CRediT authorship contribution statement

Xinyue Liu: Investigation, Methodology, Writing - original draft. **Hongwei Zhao:** Data curation, Visualization, Formal analysis. **Shan Jiang:** Investigation. **Shuai Wu:** Investigation. **Tong Zhao:** Investigation. **Lixiang Li:** Methodology, Formal analysis, Funding acquisition. **Xin Geng:** Investigation. **Haiming Yang:** Investigation. **Weimin Zhou:** Investigation. **Chengguo Sun:** Investigation. **Yiqing Chen:** Methodology. **Baigang An:** Conceptualization, Writing - review & editing, Funding acquisition.

Declaration of Competing Interest

The authors declare that they have no known competing financial interests or personal relationships that could have appeared to influence the work reported in this paper.

Acknowledgements

The financial supports from NSFC projects of No. 51672117, 51672118, 51972156, 51872131, the project of Key Research Plan of Liaoning Province, No. 2018304017 and the project of Distinguished Professor of Education Department of Liaoning Province are acknowledged.

References

[1] P. Nguyen, C. Pham, Innovative porous SiC-based materials: From nanoscopic understandings to tunable carriers serving catalytic needs, Appl. Catal. A-Gen. 391 (2011) 443–454, https://doi.org/10.1016/j.apcata.2010.07.054
[2] W.F. Seng, P.A. Barnes, Calculations of cobalt silicide and carbide formation on SiC using the Gibbs free energy, Mater. Sci. Eng. B 72 (2000) 13–18, https://doi.org/10.1016/S0921-5107(99)00586-3
[3] Y.H. Kim, Y.W. Kim, W.S. Seo, Processing and properties of silica-bonded porous nano-SiC ceramics with extremely low thermal conductivity, J. Eur. Ceram. Soc. 40 (2020) 2623–2633, https://doi.org/10.1016/j.jeurceramsoc.2019.11.072
[4] T. Remyamol, R. Gopi, M.R. Ajith, B. Pant, Porous silicon carbide structures with anisotropic open porosity for high-temperature cycling applications, J. Eur. Ceram. Soc. 41 (2021) 1828–1833, https://doi.org/10.1016/j.jeurceramsoc.2020.10.060
[5] Z.J. Wang, Y.H. Wu, M.H. Mahmud, Z. Yuan, H.A. Mantooth, Busbar design and optimization for voltage overshoot mitigation of a silicon carbide high-power three-phase T-type inverter, IEEE Trans. Power Electron. 36 (2021) 204–214, https://doi.org/10.1109/TPEL. 2020.2998465
[6] H. Ba, Y.F. Liu, X.K. Mu, W.H. Doh, J.M. Nhut, P. Granger, C. Pham-Huu, Macroscopic nanodiamonds/β-SiC composite as metal-free catalysts for steam-free dehydrogenation of ethylbenzene to styrene, Appl. Catal. A-Gen. 499 (2015) 217–226, https://doi.org/10.1016/j.apcata.2015.04.022
[7] R.L. Zhu, Q.Z. Chen, J. Du, Q.Z. He, P. Liu, Y.F. Xi, H.P. He, Organoclay-derived lamellar silicon carbide/carbon composite as an ideal support for Pt nanoparticles: facile synthesis and toluene oxidation performance, Chem. Commun. 56 (2020) 9489–9492, https://doi.org/10.1039/D0CC04187D
[8] C. Duong-Viet, J.M. Nhut, T. Truong-Huu, G. Tuci, L. Nguyen-Dinh, Y.F. Liu, C. Pham, G. Giambastiani, C. Pham-Huu, A nitrogen-doped carbon coated silicon carbide as a robust and highly efficient metal-free catalyst for sour gases desulfurization in the pesence of aromatics as contaminants, Catal. Sci. Technol. 10 (2020) 5487–5500, https://doi.org/10.1039/D0CY00945H
[9] H.L. Yu, J.Q. Zhu, L. Yang, B. Dai, L. Baraban, G. Cuniberti, J. Han, Superhydrophobic carbon nanotube/silicon carbide nanowire nanocomposites, Mater. Des. 87 (2015) 198–204, https://doi.org/10.1016/j.matdes.2015.08.025
[10] S. Li, Y. Li, C.C. Wei, P. Wang, P.L. Gao, L.J. Zhou, G.W. Wen, One step co-sintering of silicon carbide ceramic membrane with the aid of boron carbide, J. Eur. Ceram. Soc. 41 (2021) 1181–1188, https://doi.org/10.1016/j.jeurceramsoc.2020.09.065
[11] B.X. Zhang, Y.B. Zhang, Z.H. Luo, W.J. Han, W.F. Qiu, T. Zhao, Monolithic silicon carbide with interconnected and hierarchical pores fabricated by reaction-induced phase separation, J. Am. Ceram. Soc. 102 (2019) 3860–3869, https://doi.org/10.1111/jace.16263
[12] I.H. Son, J.H. Park, S. Kwon, S. Park, M.H. Rummeli, A. Bachmatiuk, H.J. Song, J. Ku, J.W. Choi, J.M. Choi, S.G. Doo, H. Chang, Silicon carbide-free graphene growth on silicon for lithium-ion battery with high volumetric energy density, Nat. Commun. 6 (2015) 7393, https://doi.org/10.1038/ncomms8393
[13] Y. Zhang, K. Hu, Y.L. Zhou, Y.B. Xia, N.F. Yu, G.L. Wu, Y.S. Zhu, Y.P. Wu, H.B. Huang, A facile, one-step synthesis of silicon/silicon carbide/carbon nanotube nanocomposite as a cycling-stable anode for lithium ion batteries, Nanomaterials 9 (2019) 1624, https://doi.org/10.3390/nano 9111624
[14] H.T. Zhang, H. Xu, Nanocrystalline silicon carbide thin film electrodes for lithium-ion batteries, Solid State Ion. 263 (2014) 23–26, https://doi.org/10.1016/j.ssi.2014.04.020
[15] Y. Zhang, K. Hu, J.H. Ren, Y.P. Wu, N.F. Yu, A.L. Feng, Z.Y. Huang, Z. Jia, G.L. Wu, A sandwich-like Si/SiC/nanographite sheet as a high performance anode for lithium-ion batteries, Dalton Trans. 48 (2019) 17683–17690, https://doi.org/10.1039/c9dt0 4228h
[16] M. Kim, I. Oh, J. Kim, Superior electric double layer capacitors using micro- and mesoporous silicon carbide sphere, J. Mater. Chem. A 3 (2015) 3944–3951, https://doi.org/10.1039/c4ta07110g
[17] A. Sanger, A. Kumar, A. Kumar, P.K. Jain, Y.K. Mishra, R. Chandra, Silicon carbide nanocauliflowers for symmetric supercapacitor devices, Ind. Eng. Chem. Res. 55 (2016) 9452–9458, https://doi.org/10.1021/acs.iecr.6b02243
[18] M. Kim, I. Oh, J. Kim, Supercapacitive behavior depending on the mesopore size of three-dimensional micro-, meso- and macroporous silicon carbide for supercapacitors, Phys. Chem. Chem. Phys. 17 (2015) 4424–4433, https://doi.org/10.1039/c4cp05357e
[19] C.H. Chang, B. Hsia, J.P. Alper, S. Wang, L.E. Luna, C. Carraro, S.Y. Lu, R. Maboudian, High-temperature all solid-state microsupercapacitors based on SiC nanowire electrode and YSZ electrolyte, ACS Appl. Mater. Interfaces 7 (2015) 26658–26665, https://doi.org/10.1021/acsami.5b08423
[20] C.H. Shih, J.S. Tulenko, R.H. Baney, Low-temperature synthesis of silicon carbide inert matrix fuel through a polymer precursor route, J. Nucl. Mater. 409 (2011) 199–206, https://doi.org/10.1016/j.jnucmat.2010.12.027
[21] C. Durif, M. Wynn, M. Balestrat, G. Franchin, Y.-W. Kim, A. Leriche, P. Miele, P. Colombo, S. Bernard, Open-celled silicon carbide foams with high porosity from boron-modified polycarbosilanes, J. Eur. Ceram. Soc. 39 (2019) 5114–5122, https://doi.org/10.1016/j.jeurceramsoc.2019.08.012
[22] N.D. Shcherban, S.M. Filonenko, P.S. Yaremov, S.A. Sergiienko, V.G. Iiyin, D.Y. Murzin, Carbothermal synthesis of porous silicon carbide using mesoporous silicas, J. Mater. Sci. 52 (2017) 3917–3926, https://doi.org/10.1007/s10853-016-0652-7
[23] H.G. Liu, S.Q. Wu, C.Y. You, N. Tian, Y. Li, N. Chopra, Recent progress in morphological engineering of carbon materials for electromagnetic interference shielding, Carbon 172 (2021) 569–596, https://doi.org/10.1016/j.carbon.2020.10.067
[24] S. Ghasemi, K. Moth-Poulsen, Single molecule electronic devices with carbon-based materials: status and opportunity, Nanoscale 13 (2021) 659–671, https://doi.org/10.1039/d0nr07844a
[25] Y. Yuan, Z. Chen, H.X. Yu, X.K. Zhang, T.T. Liu, M.T. Xia, R.T. Zheng, M. Shui, J. Shu, Heteroatom-doped carbon-based materials for lithium and sodium ion batteries, Energy Storage Mater. 32 (2020) 65–90, https://doi.org/10.1016/j.ensm.2020.07.027
[26] Q. Lu, B. Lu, M.F. Chen, X.Y. Wang, T. Xing, M.H. Liu, X.Y. Wang, Porous activated carbon derived from Chinese-chive for high energy hybrid lithium-ion capacitor, J. Power Sources 398 (2018) 128–136, https://doi.org/10.1016/j.jpowsour.2018.07.062
[27] S.J. Wang, R.T. Wang, Y.B. Zhang, L. Zhang, Highly porous carbon with large electrochemical ion absorption capability for high-performance supercapacitors and ion capacitors, Nanotechnology 28 (2017) 445406, https://doi.org/10.1088/1361-6528/aa848a
[28] T.Y. Liu, G.L. Liu, Block copolymer-based porous carbons for supercapacitors, J. Mater. Chem. A 7 (2019) 23476–23488, https://doi.org/10.1039/c9ta07770g
[29] M. Xu, Q. Yu, Z.H. Liu, J.S. Lv, S. Lian, B. Hu, L.Q. Mai, L. Zhou, Tailoring porous carbon spheres for supercapacitors, Nanoscale 10 (2018) 21604–21616, https://doi.org/10.1039/c 8nr07560c
[30] T.Y. Liu, F. Zhang, Y. Song, Y. Li, Revitalizing carbon supercapacitor electrodes with hierarchical porous structures, J. Mater. Chem. A 5 (2017) 17705–17733, https://doi.org/10.1039/c7ta05646j
[31] X.W. Liu, T.J. Sun, J.L. Hu, S.D. Wang, Composites of metal-organic frameworks and carbon-based materials: preparations, functionalities and applications, J. Mater. Chem. A 4 (2016) 3584–3616 https://doi.org/10.1039.C5TA09924B.
[32] B. Mclean, C.A. Eveleens, I. Mitchell, G.B. Webber, A.J. Page, Catalytic CVD synthesis of boron nitride and carbon nanomaterials-synergies between experiment and theory, Phys. Chem. Chem. Phys. 39 (2017) 26466–26494, https://doi.org/10.1039/C7CP0 3835F
[33] J. Plutnar, M. Pumera, Z. Sofer, The chemistry of CVD graphene, J. Mater. Chem. C 23 (2018) 6082–6101, https://doi.org/10.1039/C8TC00463C
[34] J.B. Liu, Y. Xue, S. Han, Ionic-liquid-assisted synthesis of nitrogen-doped porous carbon for high-performance supercapacitors, J. Alloy. Compd. 806 (2019) 1542–1549, https://doi.org/10.1016/j.jallcom.2019.07.151
[35] L. Fang, Y.P. Xie, Y.Y. Wang, Z.W. Zhang, P. Liu, N. Cheng, J.F. Liu, Y.C. Tu, H.B. Zhao, J.J. Zhang, Facile synthesis of hierarchical porous carbon nanorods for supercapacitors application, Appl. Surf. Sci. 464 (2019) 479–487, https://doi.org/10.1016/j.apsusc.2018.09.124

[36] Q.L. Zhao, X.Y. Wang, J. Liu, H. Wang, Y.W. Zhang, J. Gao, Q. Lu, H.Y. Zhou, Design and synthesis of three-dimensional hierarchical ordered porous carbons for supercapacitors, Electrochim. Acta 154 (2015) 110–118, https://doi.org/10.1016/j.electacta.2014.12.052
[37] G. Hasegawa, K. Kanamori, T. Kiyomura, H. Kurata, T. Abe, K. Nakanishi, Hierarchically porous carbon monoliths comprising ordered mesoporous nanorod assemblies for high-voltage aqueous supercapacitors, Chem. Mater. 28 (2016) 3944–3950, https://doi.org/10.1021/acs.chemmater.6b01261
[38] L.Z. Liu, G. Zeng, J.X. Chen, L.L. Bi, L.M. Dai, Z.H. Wen, N-doped porous carbon nanosheets as pH-universal ORR electrocatalyst in various fuel cell devices, Nano Energy 49 (2018) 393–402, https://doi.org/10.1016/j.nanoen.2018.04.061
[39] B.G. An, S.F. Xu, L.X. Li, J. Tao, F. Huang, X. Geng, Carbon nanotubes coated with a nitrogen-doped carbon layer and its enhanced electrochemical capacitance, J. Mater. Chem. A 1 (2013) 7222–7228, https://doi.org/10.1039/c3ta10830a
[40] Z.Q. Zhao, S. Das, G.L. Xing, P. Fayon, P. Heasman, M. Jay, S. Bailey, C. Lambert, H. Yamada, T. Wakihara, A. Trewin, T. Ben, S. Qiu, V. Valtchev, A 3D organically synthesized porous carbon material for lithium-ion batteries, Angew. Chem.-Int. Ed (2018) 11952–11956, https://doi.org/10.1002/anie.201805924
[41] H.W. Zhao, T.Y. Xing, L.X. Li, X. Geng, K. Guo, C.G. Sun, W.M. Zhou, H.M. Yang, R.F. Song, B.G. An, Synthesis of cobalt and nitrogen co-doped carbon nanotubes and its ORR activity as the catalyst used in hydrogen fuel cells, Int. J. Hydrog. Energy 44 (2019) 25180–25187, https://doi.org/10.1016/j.ijhydene.2019.03.271
[42] H.W. Zhao, L.X. Li, Y.Y. Liu, X. Geng, H.M. Yang, C.G. Sun, B.G. An, Synthesis and ORR performance of nitrogen-doped ordered microporous carbon by CVD of acetonitrile vapor using silanized zeolite as template, Appl. Surf. Sci. 504 (2020) 144438, https://doi.org/10.1016/j.apsusc.2019.144438
[43] H.M. Chiang, K.Y. Cho, L.X. Zeng, H.L. Chiang, Characteristics of carbon material formation on SBA-15 and Ni-SBA-15 templates by acetylene decomposition and their bioactivity effects, Materials 9 (2016) 350, https://doi.org/10.3390/ma9050350
[44] Z.P. Chen, W.C. Ren, L.B. Gao, B.L. Liu, S.F. Pei, H.M. Cheng, Three dimensional flexible and conductive interconnected graphene networks grown by chemical vapour deposition, Nat. Mater. 10 (2011) 424–428, https://doi.org/10.1038/nmat3001
[45] H.W. Zhao, Y.Q. Zhang, L.X. Li, X. Geng, H.M. Yang, W.M. Zhou, C.G. Sun, B.G. An, Synthesis of an ordered porous carbon with the dual nitrogen-doped interfaces and its ORR catalysis performance, Chin. Chem. Lett. 32 (2021) 140–145, https://doi.org/10.1016/j.cclet.2020.11.035
[46] B. Zhao, H.J. Zhang, H.H. Tao, Z.J. Tan, Z. Jiao, M.H. Wu, Low temperature synthesis of mesoporous silicon carbide via magnesiothermic reduction, Mater. Lett. 65 (2011) 1552–1555, https://doi.org/10.1016/j.matlet.2011.02.075
[47] P.C. Gao, Y. Lei, A.F.C. Perez, K. Rajoua, F. Favier, New topotactic synthetic route to mesoporous silicon carbide, J. Mater. Chem. 21 (2011) 15798–15805, https://doi.org/10.1039/c1jm12457a
[48] F. Di, N. Wang, L.X. Li, X. Geng, H.M. Yang, W.M. Zhou, C.G. Sun, B.G. An, Coral-like porous composite material of silicon and carbon synthesized by using diatomite as self-template and precursor with a good performance as anode of lithium-ions battery, J. Alloy. Compd. 854 (2021) 157253, https://doi.org/10.1016/j.jallcom.2020.157253
[49] Z.H. Bao, M.R. Weatherspoon, S. Shian, Y. Cai, P.D. Graham, S.M. Allan, G. Ahmad, M.B. Dickerson, B.C. Church, Z.T. Kang, H.W. Abernathy, C.J. Summers, M.L. Liu, K.H. Sandhage, Chemical reduction of three-dimensional silica micro-assemblies into microporous silicon replicas, Nature 446 (2007) 172–175, https://doi.org/10.1038/nature05570
[50] J. Ahn, H.S. Kim, J. Pyo, J.K. Lee, Variation in crystalline phases: controlling the selectivity between silicon and silicon carbide via magnesiothermic reduction using silica/carbon composites, Chem. Mater. 28 (2016) 1526–1536, https://doi.org/10.1021/acs.chemmater.5b05037
[51] Z.H. Liu, W.H. Shen, W.B. Bu, H.G. Chen, Z.L. Hua, L.X. Zhang, L. Li, J.L. Shi, S.H. Tan, Low-temperature formation of nanocrystalline β-SiC with high surface area and mesoporosity via reaction of mesoporous carbon and silicon powder, Microporous Mesoporous Mater. 82 (2005) 137–145, https://doi.org/10.1016/j.micromeso.2005.02.022
[52] T. Kaneko, D. Nemoto, A. Horiguchi, N. Miyakawa, FTIR analysis of a-SiC:H films grown by plasma enhanced CVD, J. Cryst. Growth 275 (2005) 1097–1101, https://doi.org/10.1016/j.jcrysgro.2004.11.128
[53] Y. Fang, P.S.J. Lakey, S. Riahi, A.T. McDonald, M. Shrestha, D.J. Tobias, M. Shiraiwa, V.H. Grassian, A molecular picture of surface interactions of organic compounds on prevalent indoor surfaces: limonene adsorption on SiO_2, Chem. Sci. 10 (2019) 2906–2914, https://doi.org/10.1039/c8sc05560b
[54] J. Percino, J. Pacheco, G. Soriano-Moro, M. Ceron, M.E. Castro, V. Chapela, J. Bonilla-Cruz, T. Lara-Ceniceros, M. Flores-Guerrero, E. Saldivar-Guerra, Synthesis, characterization and theoretical calculations of model compounds of silanols catalyzed by TEMPO to elucidate the presence of Si–O–Si and Si–O–N bonds, RSC Adv. 5 (2015) 79829–79844, https://doi.org/10.1039/c5ra10056a
[55] T.Q. Lin, I.W. Chen, F.X. Liu, C.Y. Yang, H. Bi, F.F. Xu, F.Q. Huang, Nitrogen-doped mesoporous carbon of extraordinary capacitance for electrochemical energy storage, Science 350 (2015) 1508–1513, https://doi.org/10.1126/science.aab3798
[56] J. Wei, D.D. Zhou, Z.K. Sun, Y.H. Deng, Y.Y. Xia, D.Y. Zhao, A controllable synthesis of rich nitrogen-doped ordered mesoporous carbon for CO_2 capture and supercapacitors, Adv. Funct. Mater. 23 (2013) 2322–2328, https://doi.org/10.1002/adfm.2 01202764
[57] Y.H. Deng, J. Wei, Z.K. Sun, D.Y. Zhao, Large-pore ordered mesoporous materials templated from non-Pluronic amphiphilic block copolymers, Chem. Soc. Rev. 42 (2013) 4054–4070, https://doi.org/10.1039/C2CS35426H
[58] W. Zhou, F.F. Sun, K. Pan, G.H. Tian, B.J. Jiang, Z.Y. Ren, C.G. Tian, H.G. Fu, Well-ordered large-pore mesoporous anatase TiO2 with remarkably high thermal stability and improved crystallinity: preparation, characterization, and photocatalytic performance, Adv. Funct. Mater. 21 (2011) 1922–1930, https://doi.org/10.1002/adfm. 201002535
[59] G.X. Xin, Y.H. Wang, S.P. Jia, P.F. Tian, S.Y. Zhou, J.B. Zang, Synthesis of nitrogen-doped mesoporous carbon from polyaniline with an F127 template for high-performance supercapacitors, Appl. Surf. Sci. 442 (2017) 654–660, https://doi.org/10.1016/j.apsusc.2017.06.084
[60] B.B. Liu, L. Liu, Y.F. Yu, Y. Zhang, A.B. Chen, Synthesis of mesoporous carbon with tunable pore size for supercapacitors, New J. Chem. 44 (2020) 1036–1044, https://doi.org/10.1039/C9NJ05085J
[61] N. Talrejaa, S.H. Jung, L.T.H. Yen, T.Y. Kim, Phenol-formaldehyde-resin-based activated carbons with controlled pore size distribution for high-performance supercapacitors, Chem. Eng. J. 379 (2020) 122332, https://doi.org/10.1016/j.cej.2019.122332
[62] Y.L. Shao, M.F. EL-Kady, J.Y. Sun, Y.G. Li, Q.H. Zhang, M.F. Zhu, H.Z. Wang, B. Dunn, R.B. Kaner, Design and mechanisms of asymmetric supercapacitors, Chem. Rev. 118 (2018) 9233–9280, https://doi.org/10.1021/acs.chemrev.8b00252
[63] K.M. Ajay, M.N. Dinesh, Performance studies of bamboo based nano activated carbon electrode material for supercapacitor applications, Mater. Today.: Proc. (2020), https://doi.org/10.1016/j.matpr.2020.09.691
[64] E. Taer, D.A. Yusra, A. Amri, R. Taslim, A. Putri, The synthesis of activated carbon made from banana stem fibers as the supercapacitor electrodes, Mater. Today.: Proc. (2021), https://doi.org/10.1016/j.matpr.2020.11.645
[65] C.K. Roy, S.S. Shah, A.H. Reaz, S. Sultana, A.N. Chowdhury, S.H. Firoz, M.H. Zahir, M.A.A. Qasem, M.A. Aziz, Preparation of hierarchical porous activated carbon from banana leaves for high-performance supercapacitor: effect of type of electrolytes on performance, Chem. Asian J. 15 (2021) 296–308, https://doi.org/10.1002/asia.202001342
[66] E. Taer, N. Yanti, W.S. Mustika, A. Apriwandi, R. Taslim, A. Agus, Porous activated carbon monolith with nanosheet/nanofiber structure derived from the green stem of cassava for supercapacitor application, Int. J. Energy Res. 44 (2020) 10192–10205, https://doi.org/10.1002/er.5639